SCIEPublish

Article

Side Chain Piperidinium Functionalized AEMs with an Ethylene Oxide Spacer for Improving Ion Conductivity and Alkaline Stability

Sara Gjoshi and Valadoula Deimede *

Department of Chemistry, University of Patras, GR-26504 Patras, Greece; saragjoshich@gmail.com (S.G.)

* Corresponding author. E-mail: deimede@upatras.gr (V.D.)

Received: 6 August 2025; Accepted: 15 September 2025; Available online: 23 September 2025

ABSTRACT: In this work, grafting alkaline stable piperidinium cations via ethylene oxide (EO) spacers onto an aryl ether-free poly(oxindole terphenylene) backbone was adopted as a strategy for designing self-aggregating side chain AEMs with optimized alkaline stability. Aryl ether-free poly(oxindole terphenylene) backbones were synthesized via superacid-catalyzed step-growth polycondensation and were subsequently functionalized with either piperidinium containing hydrophilic, dipolar EO or hydrophobic alkyl spacer, aiming to explore the effect of side chain-engineering on conductivity and alkaline stability of the resulting AEMs. The AEM membrane containing dipolar ethylene oxide spacer, despite its lower ion exchange capacity (IEC), exhibited a more pronounced microphase separated morphology as evidenced by TEM, and higher ionic conductivity (reaching up to 30.5 mS cm^{-1} at 80 °C) compared to the hydrophobic alkyl spacer-containing AEM membrane. This was attributed to its higher water uptake stemming from the EO hydrophilic nature and the formation of interconnected ion-conducting channels due to piperidinium–EO interactions. Additionally, the hydrophilic nature of the ethylene oxide groups endowed the membrane with enhanced alkaline stability, preserving its mechanical integrity and retaining 71.5% of its initial conductivity after 3 weeks of immersion in 2 M KOH at 80 °C. In contrast, the AEM with an alkyl spacer experienced severe degradation under the same conditions. These results suggest that incorporating flexible alkoxy-containing spacers onto an aryl ether-free backbone is a promising and simple route for fabricating mechanically and chemically robust AEMs with sufficient conductivity.

Keywords: Anion exchange membranes (AEMs); Alkaline water electrolysis; Ethylene oxide; Piperidinium; Ionic conductivity; Alkaline stability

1. Introduction

The transition towards sustainable energy systems has been an ongoing discussion for decades, with the primary motivation being the urgent need to reduce greenhouse gas emissions and replace fossil fuels for power generation in the transportation and the industrial sectors with a renewable energy carrier [1,2]. Green hydrogen has been long recognized as a promising zero-carbon energy carrier, as it can be produced from renewable energy sources using low-temperature water electrolysis [3–5]. Among low-temperature water electrolysis technologies, proton exchange membrane water electrolysis (PEMWE) is an attractive technology that delivers high hydrogen production rates at high efficiency by employing a dense proton exchange membrane (PEM) [6,7]. However, using platinum and iridium as expensive and scarce catalysts limits their large-scale implementation [8]. As a viable alternative, anion exchange membrane water electrolysis (AEMWE) can use low cost, non-platinum metal catalysts under alkaline operation, thus favoring broader applicability [9]. A key component of AEMWE is the anion exchange membrane (AEM), a cation-functionalized solid polymer electrolyte that serves a dual role in conducting hydroxide ions and preventing hydrogen permeation. The development of high performance and durable AEMWE requires robust AEMs with superior alkaline stability, high hydroxide conductivity, and dimensional stability. However, despite the great advancement, AEMs continue encountering significant challenges of insufficient conductivity and inferior long-term stability compared to PEMs [9–11].

Various strategies have been proposed to address inadequate hydroxide conductivity in AEMs stemming from the limited mobility of OH^- ions. Although ion exchange capacity (IEC) can somewhat promote conductivity, increasing

https://doi.org/10.70322/spe.2025.10010

the number of cationic groups often leads to excessive water uptake and thus swelling, adversely affecting dimensional and mechanical stability. An alternative strategy to improve the conductivity is constructing continuous OH^- conducting paths via the design of well-organized polymer architectures, such as block [12], comb/grafted shaped [13], and side-chain-type ones [14,15]. Introducing long alkyl side chains onto the polymer backbone induces hydrophilic/hydrophobic microphase separation, enabling fast ion conduction, without compromising mechanical properties. The creation of cation-dipole interactions by grafting polar poly(ethylene glycol) (PEG) or oligo (ethylene glycol) (OEG) chains as spacers between cations and polymer backbone facilitates the formation of interconnected highways for fast ion conduction owing to the regulation of the self-assembled morphology of the resulting AEMs [16–18]. For instance, Zhang et al. synthesized a series of OEG-functionalized poly(terphenyl piperidinium) polymers with varying OEG side-chain length and showed that the shorter OEG chains facilitated hydroxide conductivity due to favorable microphase separation [19]. In another work, the concept of self-aggregating cationic chains with dipolar EO spacers and alkaline stable piperidinium cations yielded AEMs with high hydroxide (106 mS cm^{-1} at 80 °C) and improved alkaline stability [20].

The second challenge lies in enhancing the chemical stability under harsh alkaline conditions, which is closely correlated with the chemical structure of the polymer backbone and the fixed cationic groups. Considering cationic groups, as reported by Marino and Kreuer, cyclic quaternary ammonium (QA) cations, including N,N-dimethyl piperidinium are exceptionally more stable than other cationic groups due to the inherent ring geometric constraints restraining the unfavorable Hoffman elimination and nucleophilic substitution degradation [21]. As for polymeric backbones, aryl ether based polyaromatics (e.g., poly(phenylene oxide), poly(aryl ether sulfone), poly(aryl ether ketone)) are the most used due to their easy preparation. However, when tethered electron-withdrawing cationic groups to aryl ether based backbones, cleavage of aryl ether linkages occurs under harsh alkaline conditions, thus leading to conductivity and mechanical integrity deterioration [22]. Therefore, AEM chemistries based on all-carbon aromatic backbones, including polyphenylenes, polystyrenes, polyfluorenes, and the more recent poly(oxindole biphenylene)s have been developed to address the limited stability of AEM based on aryl ether backbones under highly alkaline conditions [23–27]. In particular, superacid-catalyzed polyhydroxyalkylation has become a cost-effective synthetic route to get high-molecular-weight, aryl ether-free polyaromatics that can be easily functionalized with cationic groups to yield high-performance AEMs, without requiring palladium catalysts [25–29]. For example, He et al. prepared a series of poly (isatin-co-biphenyl alkylene) copolymers bearing pendant cationic groups and hydrophobic fluorinated side chains, which showed excellent alkaline resistance, retaining 90.8% of its ionic conductivity after 1560 h in 1 M KOH solution at 80 °C, and the highest current density of 4.7 A cm^{-2} at 2 V under electrolysis testing [30]. Wang et al. synthesized piperidinium-functionalized poly(biphenyl indole) containing hexyl spacers exhibiting excellent alkali resistance for 1000 h of treatment in 1 M KOH at 80 °C [31].

In this work, grafting polar ethylene oxide (EO) chains as spacers between alkali resistant piperidinium cations and poly(oxindole terphenylene) backbone was used as a strategy for the synthesis of mechanically robust AEMs with high alkaline stability and sufficient ionic conductivity. In particular, the backbone was chosen due to its aryl ether-free nature [27,29,31–35], while the introduction of EO spacers ensures the formation of cation-dipole interactions that promote dimensional stability (act as non-covalent cross-linkers), microphase separation via self-assembly, thus enabling the formation of interconnected highways for fast ion conduction, and alkali resistance improvement. The electron-donating EO groups can contribute in weakening the electropositivity of the connected cationic groups, thus limiting the OH^- attack and improving the ion dissociation. In addition, these groups can facilitate water or OH^- transport via H-bond network formation [20]. The AEM containing piperidinum side cationic groups and hydrophobic alkyl spacer was also synthesized for comparison reasons. To that end, a series of ether-free poly(oxindole terphenylene)s were synthesized via a superacid-catalyzed polycondensation reaction and modified with either piperidinium containing hydrophilic EO or hydrophobic alkyl spacer to yield the respective AEMs. The effect of the nature of side chains on key AEM properties, including water and electrolyte uptake, swelling, membrane morphology, ion conductivity, and alkaline stability, was investigated in detail.

2. Materials and Methods

2.1. Materials

Isatin (98%, Alfa Aesar, Ward Hill, MA, USA), p-terphenyl (99%, Alfa Aesar), 1,3-dibromoacetone (95%, Alfa Aesar), trifluoromethanesulfonic acid (TFSA, 99%, Fluorochem, Hadfield, UK), N-methyl piperidine (99%, Alfa Aesar), 1,5 dibromopentane (98%, Alfa Aesar), 1,2-bis(2-chloroethoxy)ethane (98%, Alfa Aesar), sodium iodide (99%,

Alfa Aesar), Sodium thiosulfate (98.5%, Sigma Aldrich, Burlington, MA, USA), anhydrous magnesium sulphate ($MgSO_4$, 99.5%, Sigma Aldrich), potassium carbonate (K_2CO_3, 99%), potassium hydroxide (+85% pellets, Merck, Darmstadt, Germany), trifluoracetic acid (TFA, 99%, Alfa Aesar), *N,N*-dimethylacetamide (DMA, 99.5%, Scharlab, Barcelona, Spain), *N,N*-dimethylformamide (DMF, 99.8%, Scharlab), N-methyl-2-pyrrolidone (NMP, 99.5%, Scharlab), acetone (≥99.5%, Scharlab), acetonitrile (CH_3CN, 99.5%, Scharlab), diethyl ether (Et_2O, ≥99%, Sigma Aldrich), dimethyl sulfoxate-d_6 (99.80 atom% Deutero DE, Kastellaun, Germany), were all used as received without further purification. Dichloromethane (DCM, Scharlab) was dried using molecular sieves.

2.2. Preparation of 1-(2-(2-(2-Iodoethoxy)ethoxy)ethyl)-methylpiperidium Iodide (I-OPip)

The synthesis of 1-(2-(2-(2-iodoethoxy)ethoxy)ethyl)-methylpiperidinium iodide (I-OPip) was conducted following a two-step procedure, as described in the literature [20]. The first step involved a Finkelstein reaction. Briefly, sodium iodide (18.5 g, 124 mmol) and 1,2-bis(2-chloroethoxy)ethane (10.65 g, 57 mmol) were added to acetone (70 mL) and heated under reflux at 80 °C for 72 h under an argon atmosphere. Subsequently, the reaction mixture was filtered to remove the precipitated NaCl by-product, and the organic phase was evaporated under reduced pressure. The crude product was dissolved in dichloromethane (DCM), and the organic phase was washed with a 15% aqueous sodium thiosulfate solution, dried over anhydrous magnesium sulfate ($MgSO_4$), and evaporated under reduced pressure. 1,2-bis(2-iodoethoxy)ethane was obtained as a viscous, pure liquid. In the final step, 1,2-Bis(2-iodoethoxy)ethane (36.9 g, 100 mmol) was dissolved in 200 mL of acetonitrile in a dry, degassed 500 mL round-bottom flask. N-Methylpiperidine (1.04 mL, 10 mmol) was then added dropwise to the reaction mixture, which was heated under reflux at 70–75 °C for 24 h under an argon atmosphere. After removal of acetonitrile under reduced pressure, the resulting oily phase was precipitated in diethyl ether, yielding a yellowish-brown solid. The product was subsequently dried under vacuum at 40 °C for 18 h. The ^{1}H NMR spectra of 1,2-bis(2-iodoethoxy)ethane and 1-(2-(2-(2-iodoethoxy)ethoxy)ethyl)-methylpiperidinium iodide are provided in Figure S1.

2.3. Preparation of 1-(5-Bromopentyl)-1-methylpiperidinium Bromide (Br-Pip)

1-(5-Bromopentyl)-1-methylpiperidinium bromide (Br-Pip) was synthesized following a similar reported procedure [34]. N-Methylpiperidine (4.86 mL, 40 mmol) was added dropwise to 220 mL acetone solution with an excess amount of 1,5 dibromopentane (54.2 mL, 400 mmol). The reaction mixture was heated under reflux for 48 h under argon atmosphere. After evaporation under reduced pressure, the oily phase was precipitated in diethyl ether to obtain the product. The product was then dried under vacuum at 40 °C for 18 h. The chemical structure of Br-Pip was characterized by ^{1}H-NMR, as depicted in Figure S2.

2.4. Synthesis of Poly(oxindole terphenylene) Copolymers P(OpTx-dBrac)

All precursor copolymers were synthesized via superacid-catalyzed step-growth polymerization, using a modified literature procedure [36,37]. Here, the synthesis of a copolymer with an isatin molar percentage of 70% is provided as an example. The monomers, p-terphenyl (0.6 g, 2.61 mmol), isatin (0.65 g, 1.69 mmol), and 1,3-dibromoacetone (0.309 g, 1.43 mmol), and dry DCM (3 mL) were added to a dry degassed 25 mL flask equipped with a magnetic stirrer. The mixture was cooled to 0–5 °C using an ice bath and stirred for 0.5 h. To avoid excessive acidification and smoke generation, TFSA (2.3 mL) was added dropwise, and the mixture was stirred vigorously at 0 °C for 50 min to obtain a highly viscous dark-blue solution. Then, it was precipitated into deionized water, yielding a white fibrous polymer. The product was thoroughly washed until it became neutral before drying overnight in a vacuum oven at 60 °C, resulting in a yield of 95%. Copolymers with varying compositions were synthesized using the same procedure, by adjusting the molar ratios of the two ketones accordingly. The synthesized copolymers are denoted as P(OpTx-dBrac), where x represents the molar percentage of the terphenyl-isatin segment (OpT) and dBrac corresponds to the 1,3-dibromoacetone monomer abbreviation.

2.5. Synthesis of Piperidinium Functionalized Poly(oxindole terphenylene) Copolymers (P(OpT70-dBrac)-OPip and P(OpT70-dBrac)-Pip)

The precursor polymer P(OpT70-dBrac) was functionalized either with I-OPip or Br-Pip, via N-alkylation in the presence of K_2CO_3 as the base, using the same procedure for both reactions. For the preparation of P(OpT70-dBrac)-OPip, precursor copolymer P(OpT70-dBrac) (0.6 g, 1.58 mmol) was fully dissolved in dry NMP (18 mL). Subsequently,

I-OPip (2.2 g, 4.74 mmol) and K_2CO_3 (0.44 g, 3.16 mmol) were added in portions under stirring. The mixture was heated to 80–85 °C under an argon atmosphere for 96 h. After completion of the reaction, the mixture was poured into a large amount of deionized water to precipitate the product, followed by thoroughly washing (with water) and drying at 60 °C overnight.

2.6. Membrane Preparation

The developed AEMs were prepared by the solution-casting method. P(OpT70-dBrac)-OPip or P(OpT70-dBrac)-Pip were dissolved in DMF to obtain a 5 wt% solution of the respective cationic polymer. The solutions were filtered through filter paper and cast onto flat glass plates at 80 °C for 24 h. Transparent and flexible membranes were then peeled off by immersing the glass plates in deionized water, followed by drying in a vacuum oven at 80 °C for 48 h. The thickness of the resulting membranes ranged from 80 to 110 μm. The membranes in the I^- and Br^- forms were soaked in 1 M KOH at room temperature for 72 h for exchanging to the OH^- form. The alkaline solution was regularly refreshed to avoid any carbonate contamination. Finally, the membranes in the OH^- form were thoroughly washed with deionized water and stored in deionized water at room temperature for further characterization.

2.7. Characterization

The proton Nuclear Magnetic Resonance (^{1}H NMR) spectra were recorded at 25 °C on an Advance DPX 600 MHz spectrometer (Bruker, Billerica, MA, USA), employing DMSO-d_6 as the solvent. A small amount of trifluoroacetic acid could be added to the functionalized polymers to shift the water peak of the deuterated solvent and to protonate any tertiary amines potentially formed during degradation after aging, thereby facilitating peak analysis. The chemical shifts are reported relative to tetramethylsilane (TMS) used as an internal standard. Attenuated Total Reflection Fourier Transform Infra-Red (ATR-FTIR) spectra were recorded on a Platinum ATR spectrometer (Bruker) in the spectral range from 4000 to 400 cm^{-1} with a resolution of 4 cm^{-1}. Thermogravimetric analysis (TGA, Labsys TG, Setaram Instrumentation, Caluire-et-Cuire, France) was performed from 25 to 800 °C under nitrogen atmosphere at a heating rate of 20 °C min^{-1}. Transmission Electron Microscopy (TEM) images were obtained using a JEM-2100 electron microscope (JEOL, Tokyo, Japan) operated at a working voltage of 120 kV. The specimen was prepared by casting an AEM thin film onto a Cu grid. Contact angle measurements were carried out by employing the sessile drop method on a static contact angle computing device (OCA 15 Plus, Data Physics Instruments, Filderstadt, Germany). Deionized water droplets (~10 μL) were pipetted onto the surface of dry membrane samples, and digital images of the droplets were captured for analysis. Contact angles were measured using the ImageJ software (version 1.54g). The average of three measurements for each sample was recorded in all cases.

2.8. Ion Exchange Capacity (IEC) of the AEMs

The theoretical IEC values of the AEMs in the Br^- and I^- form were calculated based on ^{1}H NMR data, while the corresponding values in the OH^- form were calculated assuming that all Br^- and I^- ions of the functionalized polymers were exchanged to OH^- ions. The experimental IEC was determined by Mohr's titration, as described here. Membranes in the iodide and bromide forms were first dried under vacuum at 80 °C for 24 h and weighed to obtain their dry weights. The dried membranes were then immersed in 25 mL of 1 M aqueous $NaNO_3$ solution at room temperature for 7 days to accomplish complete ion exchange. Next, 5 mL of the resulting solution was titrated with 0.01 M aqueous $AgNO_3$, and the volume consumed was recorded. A 5% aqueous K_2CrO_4 solution was used as a colorimetric indicator. The change of color indicated the titration endpoint, followed by the formation of a brown precipitate, Ag_2CrO_4. The IEC_{Br^-} or IEC_{I^-} was calculated by substituting the recorded data into the following equation:

$$\text{IEC}_{\text{Br}^-} \text{ or } \text{IEC}_{\text{I}^-} = \frac{C_{AgNO_3} \cdot V_{AgNO_3}}{m_{dry}} \ (\text{mmol g}^{-1}) \quad (1)$$

where m_{dry} (g) is the mass of the dry membranes, and the V_{AgNO3} (ml) represents the volume consumed of $AgNO_3$.

The IEC_{OH^-} was calculated (employing either IEC_{Br^-} or IEC_{I^-}) by using the following equation:

$$\text{IEC}_{\text{OH}^-} = \frac{\text{IEC}_{\text{Br}^-}}{1 - \frac{(\text{IEC}_{\text{Br}^-}) \times (M_{Br^-} - M_{OH^-})}{1000}} \ (\text{mmol g}^{-1}) \quad (2)$$

where M_{Br^-} and M_{OH^-} are the molar masses of the respective anions.

2.9. Water, Electrolyte Uptake, and Swelling Ratio

To measure the water (WU) and electrolyte uptake (EU) of the AEMs, membrane samples in their hydroxide form were first dried under vacuum at 80 °C for 24 h. After weighing, the membranes were immersed in water or 2 M aqueous KOH solution at 20 and 80 °C for 24 h. After immersion, the membranes were quickly wiped with tissue paper to remove surface water or electrolyte, and their wet weight was recorded. The water or electrolyte uptake—defined as the weight difference in the weights before (m_{dry}) and after soaking the membranes in water or electrolyte solution (m_{wet})—was calculated using the following formula:

$$\text{Water or Electrolyte uptake} = \frac{m_{wet} - m_{dry}}{m_{dry}} \times 100\ \% \tag{3}$$

The swelling ratios SR_a and SR_t were determined based on the measured area (a) and thickness (t) before (dry dimensions) and after immersion (wet dimensions) in water or 2 M KOH electrolyte solution at 20, 40, 60, and 80 °C for 24 h and calculated according to the following equations:

$$\mathrm{SR_a} = \frac{a_{wet} - a_{dry}}{a_{dry}} \times 100\% \tag{4}$$

$$\mathrm{SR_t} = \frac{t_{wet} - t_{dry}}{t_{dry}} \times 100\% \tag{5}$$

where a_{dry} and a_{wet} are the surface areas (length × width) of the dry and wet membranes, and t_{dry}, t_{wet} are the thicknesses of the dry and wet membranes, respectively.

2.10. Ionic Conductivity

The through plane ionic conductivity of AEMs was determined by AC impedance spectroscopy at 20, 40, 60, and 80 °C. A home-made Teflon cell was connected to an AUTOLAB electrochemical workstation (PGSTAT 302N, Metrohm, Dresden, Germany) equipped with a frequency response analyzer, operating over a frequency range of 10 Hz to 1000 kHz was used for conductivity measurements. The AEM membranes were placed between two perforated plate nickel electrodes of active area 4 cm^2 and sealed with two Teflon gaskets adjusted to match the doped membrane thickness to avoid mechanical failure caused by compression. The cell was filled with 2 M aqueous KOH solution. Before conductivity measurements, samples were equilibrated in 2 M KOH electrolyte solution at 80 °C for 24 h. The ionic conductivity was calculated according to Equation (6), where A corresponds to the active area of the electrodes, l represents the thickness of the doped membrane, and R denotes the ohmic resistance value between the electrodes (taken as the intercept with the real axis of the Nyquist plot).

$$\sigma = \frac{l}{A \times R} \tag{6}$$

For each membrane, two samples were prepared and measured. The average value of the two measurements was reported to ensure accuracy.

2.11. Alkaline Stability

The alkaline stability of the prepared AEMs was investigated by monitoring structural changes using ^{1}H NMR, ATR-FTIR spectroscopy, and measuring the ionic conductivity after immersion in 2 M aqueous KOH solutions at 80 °C for 3 weeks. The aging experiments were conducted in sealed PTFE vials to prevent CO_2 absorption and glass dissolution. After the designated aging period, the samples were thoroughly washed with deionized water, dried, and dissolved in DMSO-d_6 solvent containing 5–10 vol% TFA for ^{1}H NMR analysis.

3. Results and Discussion

3.1. Synthesis and Characterization of Piperidinium Functionalized Poly(oxindole terphenylene) Copolymers

To simultaneously improve ionic conductivity and alkaline stability through optimization of membrane microstructure and chemical stability, grafting alkaline stable piperidinium cations via flexible, self-aggregating ethylene oxide spacers onto a chemically robust poly(oxindole terphenylene) backbone was used as a strategy. For this reason, we designed and synthesized a series of aryl ether-free poly(oxindole terphenylene) precursor copolymers

containing dibromoacetone functional groups, followed by N-alkylation to afford the respective AEMs. The precursor copolymers were prepared via polycondensation of terphenyl, isatin, and 1,3-dibromoacetone catalyzed by TFSA (Scheme 1).

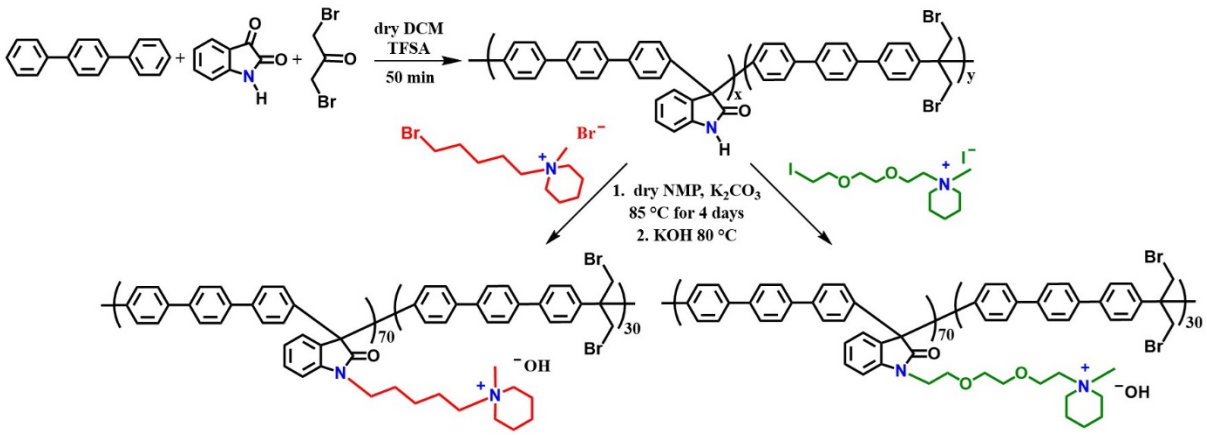

Scheme 1. Synthesis pathway for the synthesis of poly(oxindole terphenylene) precursor copolymers and their piperidinium side functionalized analogues containing either a long hydrophobic alkyl spacer (left) or long hydrophilic ethylene oxide spacer (right).

To obtain high-molecular-weight copolymers, the reaction was carried out under a slightly imbalanced stoichiometry, employing a 20% molar excess of the ketone monomers relative to the nucleophilic aromatic monomer, consistent with previously reported work [38,39]. Given the three available grafting sites in the polymer structure, two of dibromo functional groups and one site of isatin (N-H group), the initial target was to react N-methyl piperidine with dibromo sites to afford piperidinium based AEMs with sufficiently high IEC but without compromising the mechanical properties. Therefore, the molar percentage of isatin/dibromo acetone was tuned between 42/58 and 80/20, and copolymers with five different compositions were synthesized. The chemical structure of the synthesized copolymers was verified by ^{1}HNMR (DMSO-d_6 was used as a solvent) and ATR-FT-IR. Figure 1 shows the ^{1}HNMR spectra of P(OpTx-dBrac) copolymers with varying isatin molar percentage. The characteristic signal of the N-H proton in the isatin segment appeared at 10.80 ppm (**1**), while the peak at 4.55 ppm (**a**) was assigned to the methylene protons of 1,3-dibromoacetone. All the aromatic protons of the copolymers were observed between 7.0 and 7.75 ppm (**2**–**8**). The above findings confirmed successful copolymerization. The actual composition of the synthesized copolymers can be calculated by comparing the integral area of the (**a**) methylene proton peak with the isatin N-H proton.

ATR-FTIR spectroscopy further confirmed successful copolymerization (Figures 2a and S3). The broad peak located at 3380 cm^{-1} corresponds to the N-H stretching of the isatin group, while the characteristic band at 1710 cm^{-1} is assigned to the C=O stretching of the amide bond [28,29,32,34,35]. The absorption band at 2860 cm^{-1} is ascribed to the stretching vibration of –CH_2 groups of the 1,3-dibromoacetone, and the peak located at 740 cm^{-1} corresponds to C-Br stretching vibration [40].

TGA investigated the thermal stability of the prepared copolymers. As shown in Figure 2b, all copolymers displayed a two-step weight loss. The first degradation step starts at around 217 °C and is attributed to the loss of –CH_2Br groups of the 1,3-dibromoacetone moieties, while the second degradation step begins at 538 °C and results from polymer backbone decomposition. The second degradation loss is consistent with other reported ether-free polyaromatics based AEMs [28,32,34].

Regarding the solubility of the prepared copolymers, all can be easily dissolved in polar aprotic solvents such as N-methylpyrrolidone (NMP), dimethylacetamide (DMAc), and partially soluble in dimethylsulfoxide (DMSO) and dimethylformamide (DMF). As depicted in Figure S4, all copolymers with different compositions form mechanically flexible and robust transparent films upon casting from DMA.

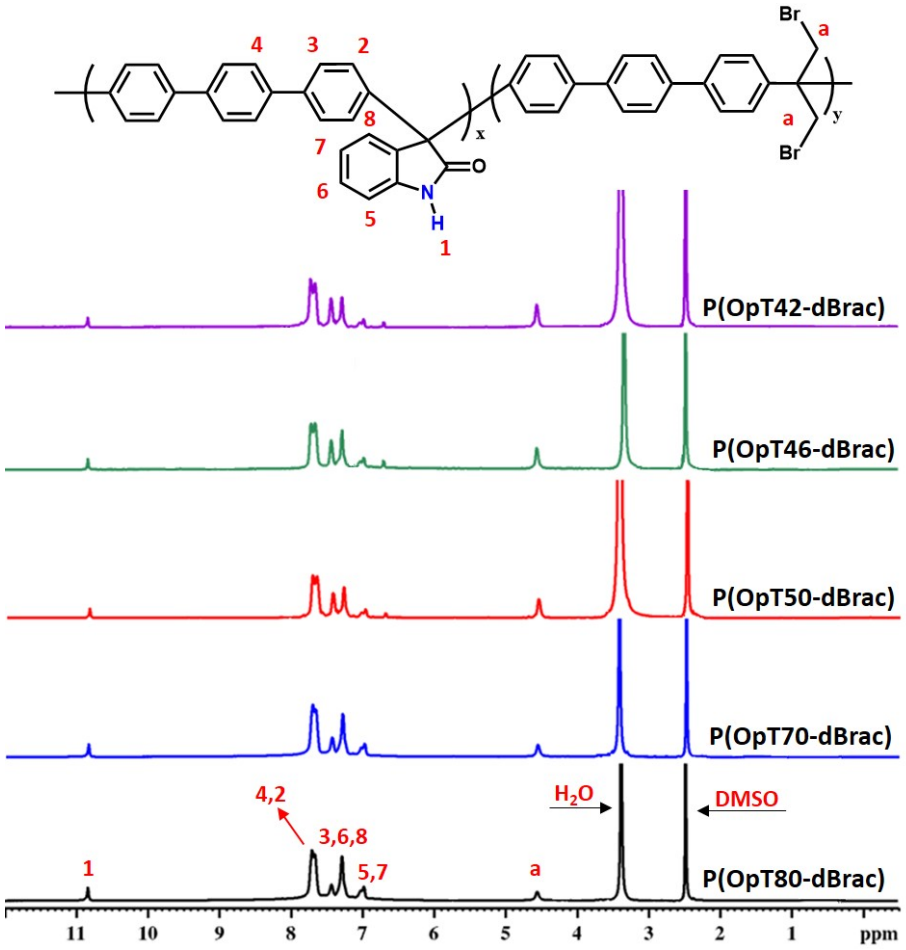

Figure 1. [1]HNMR spectra of the synthesized P(OpTx-dBrac) copolymers in DMSO-d_6.

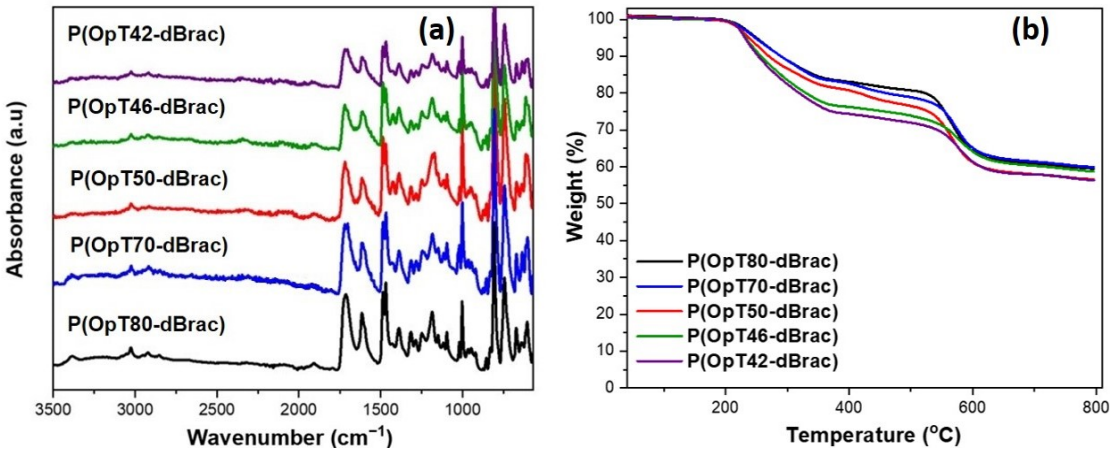

Figure 2. (**a**) ATR-FTIR spectra and (**b**) TGA curves of the P(OpTx-dBrac) copolymers with varying isatin contents.

As mentioned, functionalization of the precursor copolymers could be achieved via dibromo acetone moieties or N-H group of isatin. However, despite several trials, the dibromo functional groups could not be converted to their cationic piperidinium analogues via Menshutkin reaction with N-methyl piperidine, probably due to the sterical hindrance effects of bromine groups. Therefore, functionalization of isatin moieties of the precursor copolymer P(OpT70-dBrac) via the introduction of hydrophilic alkoxy-containing alkali-resistant piperidinium side chain was carried out to yield the AEM analogue, P(OpT70-dBrac)-OPip (Scheme 1). The copolymer with 70% isatin molar percentage was chosen to ensure high IEC and good mechanical properties. To further investigate the effect of side chain engineering, we synthesized piperidinium functionalized copolymers bearing long hydrophobic alkyl side chains as a spacer, abbreviated as P(OpT70-dBrac)-Pip (Scheme 1).

The chemical structure of functionalized copolymers with two different pendant cationic side chains was determined by recording their [1]H NMR spectra in DMSO-d_6. Comparison of the [1]HNMR spectra of P(OpT70-dBrac)-

Pip and P(OpT70-dBrac)-OPip with the precursor copolymer showed the disappearance of the characteristic signal peak at 10.80 ppm corresponding to N-H proton in the isatin segment, confirming the 100% successful functionalization of precursor with cationic side chains in both cases, as depicted in Figure 3b,c. Additionally, new chemical shifts could be observed in the 1.40–3.70 ppm range. Specifically, by taking the spectrum of P(OpT70-dBrac)-OPip as an example, two new peaks at 1.40 and 1.60 ppm emerged, ascribed to the methylene protons (**1**) and **(2**) of the piperidinium ring. The single peak at 2.90 ppm was assigned to the methyl protons (**4**) of piperidinium, while several overlapping peaks in the 3.20–3.50 ppm region were attributed to the α-protons of the piperidinium ring corresponding to methylene protons (**3**), as well as to the methylene protons (**9** and **6**) attached to oxygen groups of the flexible alkoxy side chain. The peak at 3.70 ppm corresponds to the methylene protons (**5**) of the flexible spacer adjacent to N^+ of piperidinium cation, overlapped with the methylene protons (**8** and **7**) of the flexible alkoxy spacer. The signal peak at 4.00 ppm was attributed to the methylene protons (**10**) adjacent to the nitrogen of isatin.

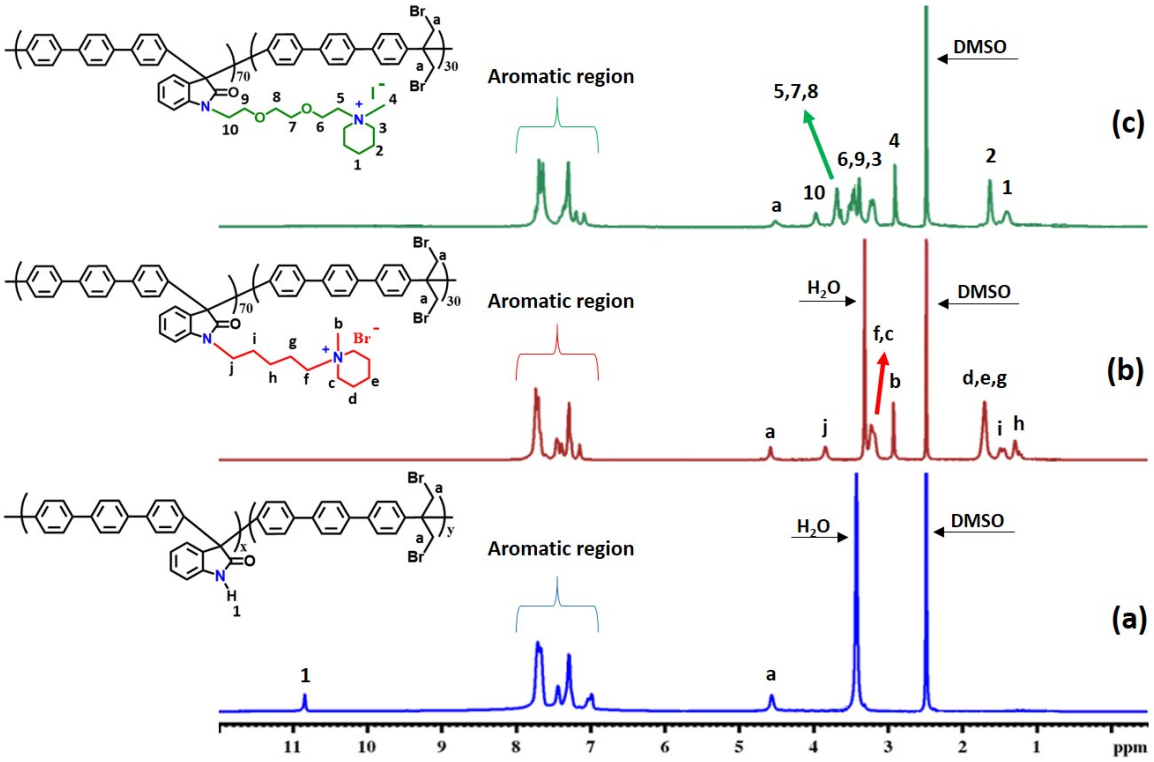

Figure 3. ^{1}HNMR spectra of (**a**) P(OpT70-dBrac) precursor copolymer, (**b**,**c**) the respective functionalized P(OpT70-dBrac)-Pip and P(OpT70-dBrac)-OPip copolymers in DMSO-*d*6. P(OpT70-dBrac)-OPip contains 5 vol% of TFA to shift the water signal to above 11 ppm.

ATR spectroscopy was also studied to verify the successful incorporation of the two different pendants onto the main chain via N-alkylation. As illustrated in Figure 4, after cationic functionalization of both copolymers, a broad peak was observed at 3400 cm^{-1}, assigned to the characteristic stretching vibration of -OH groups of water molecules, due to piperidinium hydrophilicity [41]. A new absorbance peak appeared at 2925 cm^{-1}, attributed to the stretching vibration of the methyl groups in the cationic group, while the intensity of the pre-existing peak at 2860 cm^{-1} had increased, corresponding to the stretching vibrations of methylene groups in the cationic spacer [42,43]. Furthermore, a new peak emerged at 1350 cm^{-1} corresponding to the stretching vibration of C-N^+ [28]. In the ATR spectra of P(OpT70-dBrac)-OPip, an additional absorption peak appeared at 1110 cm^{-1}, corresponding to the stretching vibration of the ether bond in the flexible alkoxy side chain [29,32]. Therefore, the appearance of these stretching vibration peaks proves the successful synthesis of the target cationic functionalized copolymers.

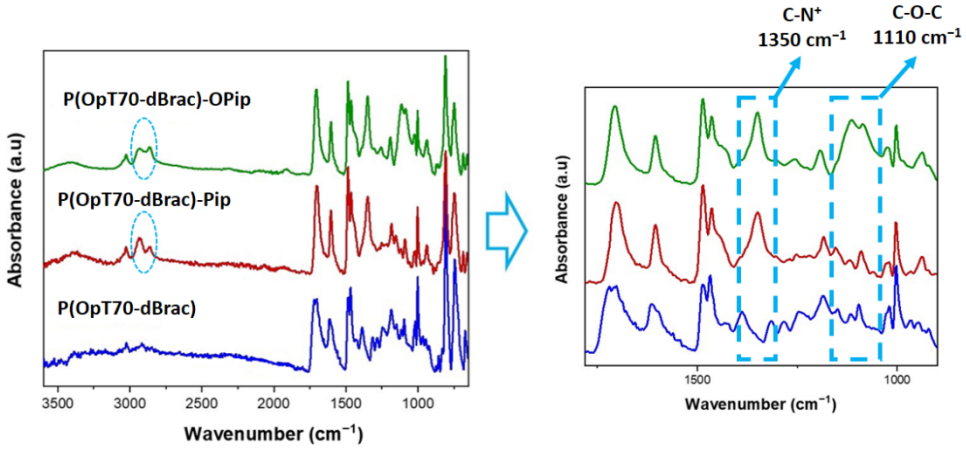

Figure 4. ATR spectra of the precursor copolymer P(OpT70-dBrac) and its functionalized derivatives P(OpT70-dBrac)-Pip and P(OpT70-dBrac)-OPip in the whole spectral region (3600–650 cm^{-1}) and the magnified region from 1800 to 900 cm^{-1}.

3.2. Thermal Stability

The thermal stability of functionalized derivatives P(OpT70-dBrac)-Pip and P(OpT70-dBrac)-OPip in bromide and iodide form was assessed through TGA under N_2 atmosphere. As shown in Figure 5, both cationic functionalized polymers exhibited a typical two-step weight loss process. For P(OpT70-dBrac)-OPip, an initial weight loss was observed between 235 and 400 °C, attributed to the thermal decomposition of both the piperidinium cationic groups and the ethylene oxide side chains, in line with previously reported EO-containing polymers and piperidinium based AEMs [26,44–47]. The second major weight loss occurring between 502 and 602 °C, corresponded to degradation of the polymer backbone. Although the precursor copolymer exhibited higher thermal stability compared to its functionalized derivatives, the resulting AEMs still demonstrated sufficient thermal robustness for application in anion exchange membrane water electrolyzers (AEMWEs).

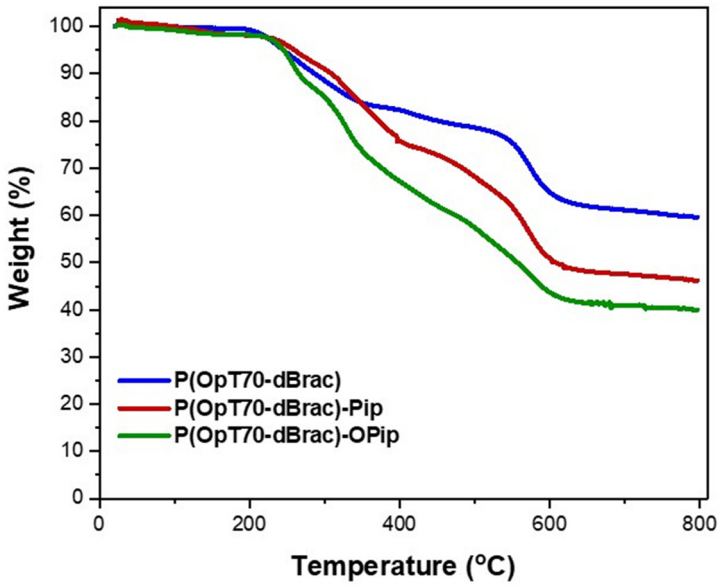

Figure 5. Comparative TGA curves of the precursor P(OpT70-dBrac) and its functionalized derivatives P(OpT70-dBrac)-Pip and P(OpT70-dBrac)-OPip.

3.3. Membrane Morphology

AEMs were prepared via solution casting of P(OpT70-dBrac)-Pip and P(OpT70-dBrac)-OPip from DMF solutions. The resulting membranes were transparent, mechanically robust, and foldable to 180° with a thickness of 80–100 μm (Figure 6a,b). The enhancement of ionic conductivity in AEMs usually arises from the formation of more efficient ion transport pathways within the membrane at the microscopic level. TEM was employed to characterize the microphase structure of the two prepared AEMs. Figure 6c and 6d present the TEM images of P(OpT70-dBrac)-Pip and P(OpT70-

dBrac)-OPip, respectively. The darker regions represent the hydrophilic domains, primarily consisting of piperidinium cations and associated water molecules, while the brighter regions correspond to hydrophobic domains composed of the aromatic polymer backbones. P(OpT70-dBrac)-OPip exhibited a more pronounced microphase-separated morphology which was attributed to the incompatibility between the hydrophilic ethylene oxide-based cationic side chains and the hydrophobic polymer backbone (Figure 6d). Specifically, the presence of flexible alkoxy spacers enhanced the cationic groups' mobility significantly, as did hydrophilicity discrimination, promoting further well-defined phase separation [20,48]. The mean diameter of the hydrophilic domains was estimated to be approximately 4.3 nm.

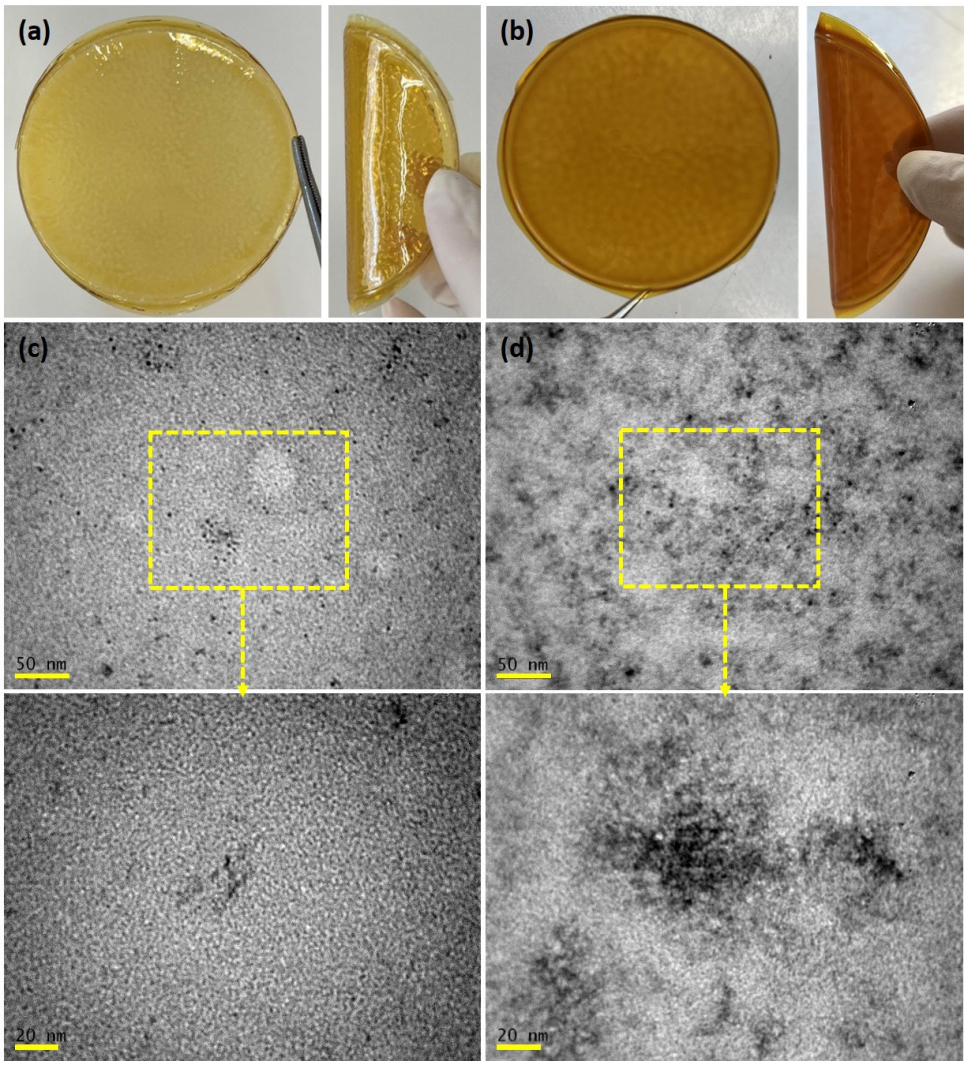

Figure 6. (**a**,**c**) Digital photographs and TEM images of P(OpT70-dBrac)-Pip membrane and (**b**,**d**) digital photographs and TEM images of P(OpT70-dBrac)-OPip membrane.

In contrast, the micro-phase separation of the P(OpT70-dBrac)-Pip membrane was much less clear due to the poor self-assembling ability (Figure 6c). Here, the ionic clusters appeared more randomly dispersed and isolated within the polymer matrix. The same behavior was also reported for other alkyl side chain type AEMs with similar backbones [15,28,34].

3.4. Ion Exchange Capacity (IEC), Water and Electrolyte Uptake and Swelling

Table 1 presents the physical properties of new synthesized AEMs P(OpT70-dBrac)-Pip and P(OpT70-dBrac)-OPip, including the IEC, water and electrolyte uptake (WU), swelling ratio (SR), contact angles, and ionic conductivity. The IEC provides the density of ion-conducting sites, through which anions are transported in the AEM. As shown in Table 1, the IEC values derived from the theoretical calculations closely matched the experimental ones measured by Mohr titration, which further confirms the high efficiency of the functionalization reactions. Specifically, the IEC experimental values were 1.32 mmol g^{-1} for P(OpT70-dBrac)-Pip and 1.24 mmol g^{-1} for P(OpT70-dBrac)-OPip in the

OH^- form. In the present study, the IECs were precisely tuned by copolymerization to reach values within a reasonable range to balance high ionic conductivity with dimensional stability.

Although a suitable level of Water Uptake (WU) in the AEMs is necessary for the formation of continuous ion-conducting channels for efficient ion transport, an excessive water uptake might result in extensive swelling and hence in compromised mechanical properties of the membranes. Therefore, the effect of side chain engineering on water uptake was studied in a wide temperature range (20 °C–80 °C) for both AEMs in hydroxide form. As expected, both membranes exhibited an increased water uptake and swelling ratio with increasing temperature (as shown in Figure S5 and Table 1). P(OpT70-dBrac)-OPip, bearing long flexible alkoxy-containing piperidinium side chains, exhibited higher water uptake (33% at 80 °C) than P(OpT70-dBrac)-Pip (20% at 80 °C), despite having a slightly lower IEC value. This increased WU is attributed to the hydrophilic nature of the ethylene oxide group spacer. The polar ethylene oxide groups provide additional sites for water absorption via H-bonding formation with water [20,45]. The water contact angle data further confirmed the more hydrophilic character of P(OpT70-dBrac)-OPip. As shown in Table 1, P(OpT70-dBrac)-OPip exhibited a relatively hydrophilic surface with a contact angle of 71.6°, whereas P(OpT70-dBrac)-Pip showed a higher contact angle of 83.4°, indicating a more hydrophobic character due to the presence of alkyl side chains, which increase the fraction of hydrophobic domains. In addition, both area swelling (18 %) and thickness swelling values (15 %) for P(OpT70-dBrac)-OPip are slightly higher than those of P(OpT70-dBrac)-Pip at 80 °C (12% and 11%, respectively). The observed low area swelling of both membranes suggests good dimensional stability compared to literature studies, which is beneficial to withstand the membrane-electrode interfacial stresses during electrolysis testing [16,49].

Table 1. Physicochemical properties of prepared AEMs.

Membrane	IEC (mmol g^{-1})		WU (%)		SR_a * (%)		SR_t * (%)		Contact Angle (°)	EU (%) [c]		σ (mS cm^{-1}) [c]
	^{1}HNMR [a]	Titration [b]	20 °C	80 °C	20 °C	80 °C	20 °C	80 °C	20 °C	20 °C	80 °C	80 °C
P(OpT70-dBrac)-Pip	1.35 (1.24)	1.32 (1.22)	15	20	6.5	12	5	11	83.4	47	72	21.5
P(OpT70-dBrac)-OPip	1.27 (1.11)	1.24 (1.09)	19	33	10	18	6	15	71.6	41	62	30.5

[a] Calculated from the ^{1}H NMR data of cationic polymers in the OH^- form (values within parenthesis correspond to Br^- and I^- form, respectively). [b] Evaluated from the titration data in the OH^- form (values within parenthesis correspond to Br^- and I^- form, respectively). [c] Measured in 2M KOH solution. * data taken in water.

Considering that AEMWEs generally operate with electrolyte solutions instead of pure water [50], AEM's ability to be doped with dilute aqueous KOH electrolyte solution plays a key role in achieving high ionic conductivity. The electrolyte uptake (EU) for the prepared cationic polymers was studied after doping in 2 M KOH solution as a function of temperature, as illustrated in Figure 7a,b and Table 1. The electrolyte uptake increased gradually with elevating temperature, following the same trend observed for WU. Specifically, both membranes displayed high electrolyte uptakes at 80 °C, corresponding to 62% and 72% for P(OpT70-dBrac)-OPip and P(OpT70-dBrac)-Pip. The slightly higher electrolyte uptake of P(OpT70-dBrac)-Pip could be attributed to its higher IEC, even though P(OpT70-dBrac)-OPip membrane, which contains hydrophilic EO spacers, would have additional sites for interactions with water and solvation of K^+ via acid-base interactions [29,32], which could further promote KOH absorption. On the other hand, the strong attractive interactions between EO groups and piperidinum (dipole-cation) may significantly hinder the interactions of EO groups with K^+, thus limiting KOH absorption.

As for the swelling ratio of KOH doped AEMs (Figure 7a,b), both exhibited low swelling area across the entire temperature range, with values of 11% and 15% for P(OpT70-dBrac)-OPip and P(OpT70-dBrac)-Pip, respectively, at 80 °C.

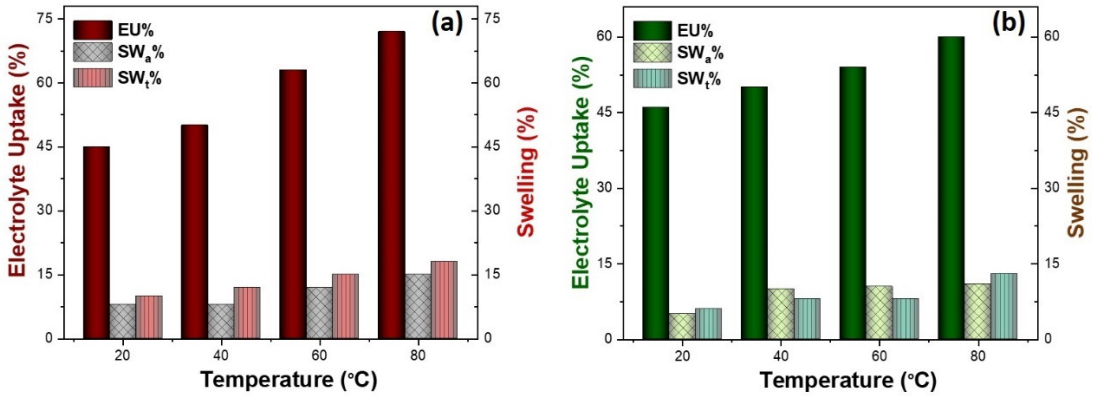

Figure 7. Electrolyte uptake and swelling behavior of (**a**) P(OpT70-dBrac)-Pip and (**b**) P(OpT70-dBrac)-OPip in 2M KOH solution as a function of temperature.

3.5. Ionic Conductivity

Ionic conductivity is a critical parameter for evaluating the performance of AEMs. Figure 8 showed the ionic conductivity of both AEMs as a function of temperature after doping in 2 M KOH solution. As temperature elevates, ion mobility is enhanced and water and electrolyte absorption increase, leading to a positive correlation between membrane conductivity and temperature. Over the entire temperature range studied, P(OpT70-dBrac)-OPip membrane displayed a higher conductivity value than P(OpT70-dBrac)-Pip membrane despite its lower IEC and EU values. Particularly, at 80 °C the former peaked around 30.5 mS cm^{-1} while the latter around 21.5 mS cm^{-1} in 2 M KOH solution. The higher conductivity can be attributed to both its higher water uptake and the cation-dipole interactions between the hydrophilic EO-containing side chains and the piperidinium moiety, enabling the formation of interconnected highways for fast ion conduction (more pronounced hydrophilic–hydrophobic microphase separation, as illustrated in Figure 6).

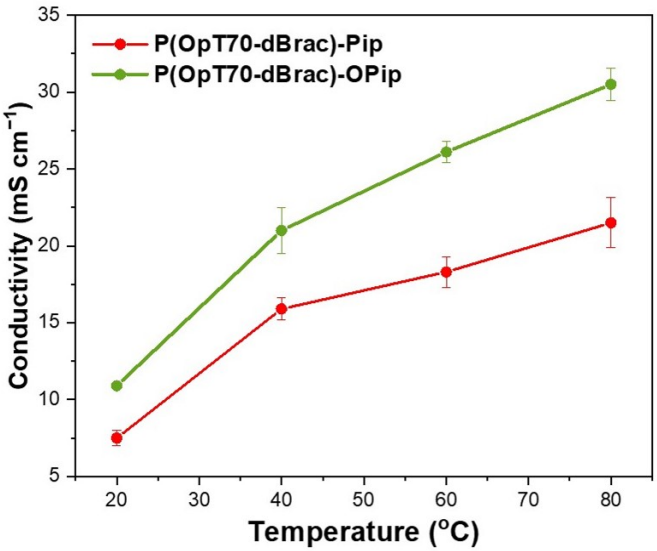

Figure 8. Ionic conductivity of AEMs in 2 M KOH solution as a function of temperature. The markers show the average of two samples and the error bars represent the standard deviation.

While AEMWE typically operates with an electrolyte solution (*i.e.*, dilute aqueous KOH) [8], most research on AEMs has predominantly focused on fuel cell applications in which the conductivity behavior is evaluated in pure water. As a result, there are limited conductivity data in dilute KOH solutions for side cationic functionalized aryl ether-free based AEMs, as mostly are recorded in pure water. For comparison, in our previous work, AEMs based on pyrrolidinium and piperidinium tethered to a poly(oxindole biphenylene) backbone with comparable IECs were developed for alkaline water electrolysis and exhibited significantly higher ionic conductivity values (81.5 mS cm^{-1} and 120 mS cm^{-1}, respectively) in 2 M KOH at 80 °C [28]. Additionally, Jannasch group, very recently, reported a series of poly(arylene piperidinium) membranes featuring two angled biphenyl units for electrochemical energy device applications, which

exhibited conductivity values between 33 and 50 mS cm^{-1} at 80 °C in 2 M aq. KOH solutions are similar to the corresponding ones of our newly synthesized AEMs [51]. The same group also synthesized polybenzimidazole functionalized with N,N-dimethylpiperidinium cations for use in dilute aqueous KOH-fed electrolyzers that displayed conductivity values in 2 M KOH at 80 °C ranging from 19 to 38 mS cm^{-1} [52].

3.6. Alkaline Stability

The strongly basic environment in AEMWE requires AEMs with high alkaline stability to ensure the long-term operational lifespan of the device. The prepared AEMs were treated in 2 M aqueous KOH at 80 °C for 3 weeks to assess their ex-situ alkaline stability by monitoring variations in ionic conductivity and chemical structure. While the P(OpT70-dBrac)-OPip membrane remained visually intact and maintained its mechanical robustness after the prolonged alkaline treatment, the P(OpT70-dBrac)-Pip membrane underwent breakage. Thus, the conductivity study could not be conducted for the aged P(OpT70-dBrac)-Pip membrane due to the loss of its mechanical strength. On the other hand, the ionic conductivity of the aged P(OpT70-dBrac)-OPip was recorded in 2 M KOH at different temperatures, as illustrated in Figure 9. Specifically, for P(OpT70-dBrac)-OPip, the decline in ionic conductivity became apparent across all temperatures, yet 71.5% of the initial conductivity (at 80 °C) was retained, indicating its high alkaline stability. In contrast, other side alkyl poly(oxindole biphenylene)-based AEMs bearing alkyl-trimethylammonium cations with hydroxyl groups in the β-position of the cationic center, showed a significant decrease in conductivity during the early stages of the alkaline stability test, even under less severe conditions. A drop of conductivity by 51% and 54 % was observed in 0.5 M and 1 M KOH solutions, respectively [53].

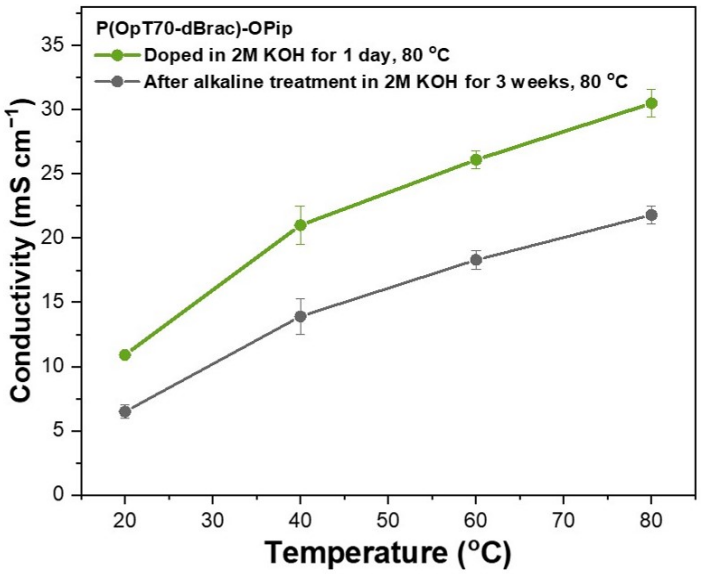

Figure 9. Ionic conductivity of the P(OpT70-dBrac)-OPip membrane during aging for 1 day and 3 weeks in 2 M KOH solution at 80 °C. The markers show the average of two samples, and the error bars represent the standard deviation.

To further investigate the origin of the conductivity loss in P(OpT70-dBrac)-OPip, as well as the severe mechanical-chemical degradation of P(OpT70-dBrac)-Pip, both aged AEMs (after washing with water and drying) were characterized using ^{1}H NMR spectroscopy in a mixed solvent (DMSO-d_6 and 5 vol% TFA). TFA was added to shift the water signal and protonate any present tertiary amines formed during degradation reactions. For P(OpT70-dBrac)-OPip, by analyzing the ^{1}H NMR spectra before and after 3 weeks' alkaline treatment (Figure 10), new degradation peaks appeared at approximately 5.05 and 5.70 ppm (small signals), corresponding to vinylic protons CH_2= and **CH**-CH_2, respectively. The appearance of these degradation peaks was attributed to the Hoffmann β-elimination reaction of the piperidinium ring (Figure 10) [28,34,51,54]. Two new signals at 9.2 and 9.1 ppm were assigned to different protonated tertiary amines, arising from ring-opening β-elimination and nucleophilic substitution, respectively [55]. Additionally, the decreased intensity of the methyl proton signal at 2.9 ppm (compared to the aromatic region intensity) further confirms the degradation of the cationic group via nucleophilic substitution. Thus, in the case of P(OpT70-dBrac)-OPip, the ^{1}HNMR data unveiled that ring-opening β-elimination and nucleophilic substitution were the main degradation pathways leading to ionic loss and subsequently to conductivity loss.

After 3 weeks of alkaline aging, P(OpT70-dBrac)-Pip membrane was only partially soluble in DMSO-d_6, likely due to cross-linking reactions [34]. However, the addition of TFA enabled complete dissolution. As shown in Figure 11, the post-aging NMR spectra exhibited all the characteristic degradation signals previously observed for P(OpT70-dBrac)-OPip, with slightly increased intensity. Notably, the additional set of signals emerged at approximately 4.9 and 5.7 ppm (corresponding to vinylic protons CH_2= and **CH**-CH_2, respectively) strongly implies that β-elimination in the alkyl spacer chain took place [28,51]. Furthermore, the new N–H signal at 10.80 ppm of the isatin segment indicated side alkyl chain cleavage, suggesting that additional degradation pathways were observed. These data confirm that the degradation of P(OpT70-dBrac)-Pip was more pronounced than that of P(OpT70-dBrac)-OPip, eventually resulting in membrane embrittlement (inset photograph of Figure 11). The proposed degradation products of both AEMs are illustrated in Figures 10 and 11, respectively.

The enhanced alkaline resistance of AEM containing flexible side EO spacers compared to that of the AEM with alkyl spacers is attributed to the presence of hydrophilic and electron–donating EO spacers, which reduce the possibility of OH^- attack on piperidinium cations, according to literature [17,20,45,48]. In particular, the hydrophilicity of ethylene oxide groups enables the dilution of local KOH concentration close to piperidinium due to the enhanced water uptake, thus mitigating the degradation of piperidinium. In addition, piperidinium groups are more protected against OH^- attack due to both sterical hindrance induced by the bulky hydrated OE chains and reduced electropositivity owing to the electron-donating properties of the EO group [20]. Finally, it should be stated that dipole –cation interactions promote not only alkaline stability but mechanical robustness as well. Therefore, the P(OpT70-dBrac)-OPip membrane possesses sufficiently high mechanical and chemical robustness after aging.

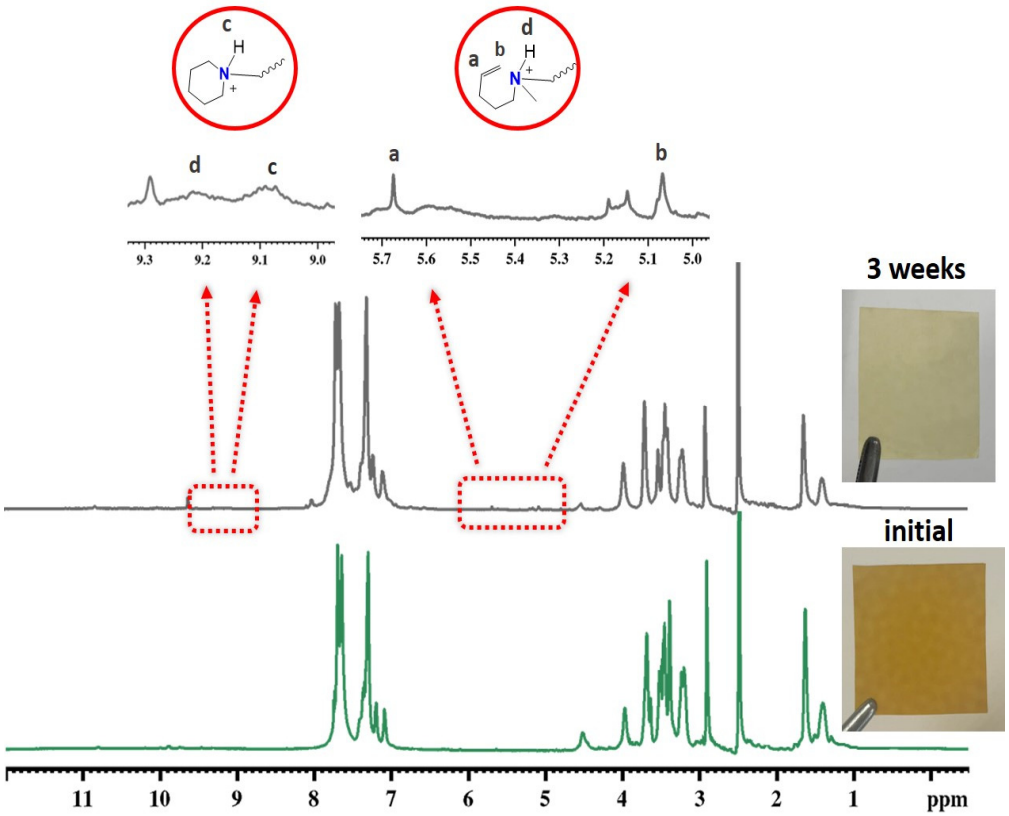

Figure 10. ^{1}H NMR spectra of P(OpT70-dBrac)-OPip before and after storage in 2 M KOH for 3 weeks at 80 °C.

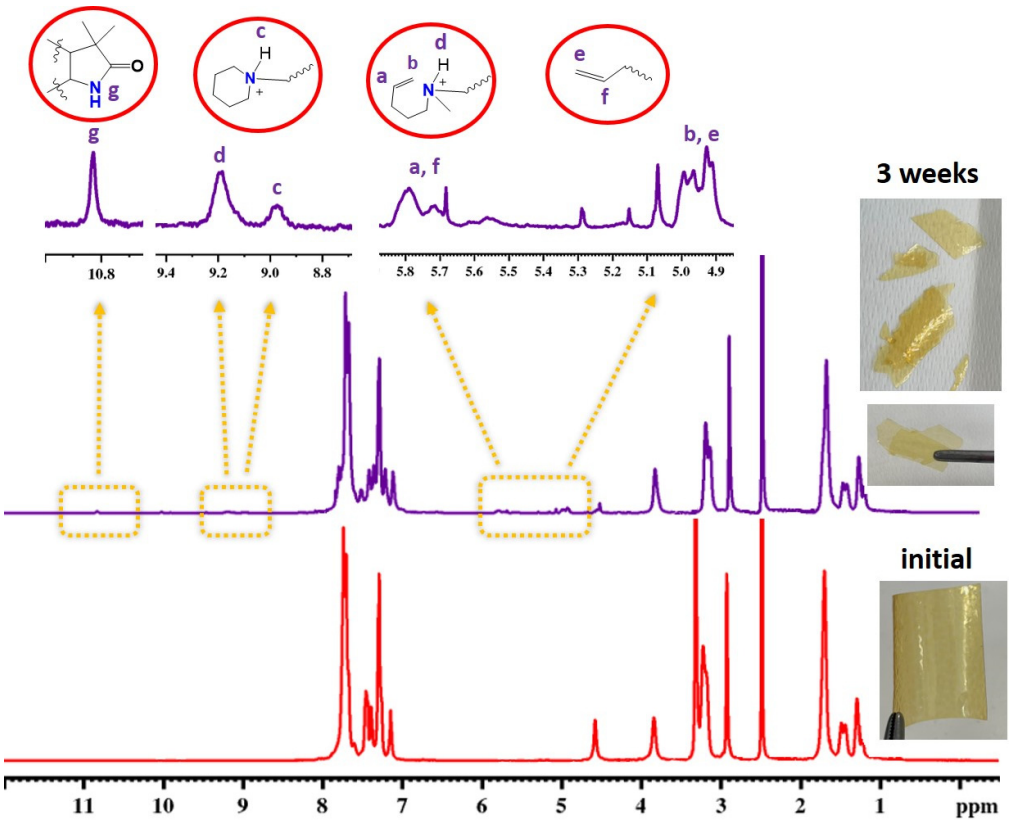

Figure 11. ^{1}H NMR spectra of P(OpT70-dBrac)-Pip before and after storage in 2 M KOH for 3 weeks at 80 °C.

The aged samples were also analyzed by ATR spectroscopy as a complement to the ^{1}H NMR study. A comparison of the ATR-IR spectra before and after aging for both AEMs (Figure S6 and Figure S7, for P(OpT70-dBrac)-OPip and P(OpT70-dBrac)-Pip, respectively) did not provide more information regarding the potential degradation of AEMs, as no new signal peaks indicative of degradation of piperidinium or C2 carbonyl group of isatin emerged.

4. Conclusions

In summary, we designed a series of new aryl ether-free poly(oxindole terphenylene) copolymers functionalized with two distinct cationic side-chain architectures. The precursor copolymers were synthesized via Friedel–Crafts polyhydroxyalkylation, followed by post-functionalization with either long alkyl chain or hydrophilic ethylene oxide (EO)-containing piperidinium pendants. The resultant AEM membranes achieved high electrolyte uptake values of 72% for P(OpT70-dBrac)-Pip and 62% for P(OpT70-dBrac)-OPip. The incorporation of hydrophilic EO groups in P(OpT70-dBrac)-OPip induced a more pronounced microphase-separated structure, enabling the formation of ion-conducting channels, as evidenced by TEM. Despite its lower IEC compared to P(OpT70-dBrac)-Pip, the P(OpT70-dBrac)-OPip membrane displayed higher water uptake (33% at 80 °C) and superior ionic conductivity (30.5 mS cm^{-1} at 80 °C). The latter was attributed to its higher water uptake and the favorable phase-separated morphology facilitated by dipolar interactions between the EO side chains and piperidinium groups. In addition, ex situ alkaline stability tests (2 M KOH at 80 °C for 3 weeks) revealed that P(OpT70-dBrac)-OPip exhibited improved alkaline stability, retaining its mechanical integrity and 71.5% of its initial ionic conductivity at 80 °C. The observed conductivity loss was primarily attributed to cationic degradation via ring-opening β-elimination and nucleophilic substitution mechanisms. In contrast, P(OpT70-dBrac)-Pip underwent significant degradation via additional degradation pathways, losing its mechanical integrity under alkaline conditions.

Supplementary Materials

The following supporting information can be found at: https://www.sciepublish.com/article/pii/688, Figure S1: ^{1}H NMR spectra of (a) 1,2-bis (2-iodoethoxy)ethane and (b) 1-(2-(2-(2-iodoethoxy)ethoxy)ethyl)-methylpiperidinium iodide (I-OPip); Figure S2: ^{1}H NMR spectra of Br-Pip; Figure S3: ATR-FTIR spectrum of the P(OpT80-dBrac) copolymer; Figure S4: Photographs of synthesized P(OpTx-dBrac) copolymers; Figure S5: Water uptake and swelling behavior of (a) P(OpT70-dBrac)-Pip and (b) P(OpT70-dBrac)-OPip in the OH^{-} form as a function of temperature;

Figure S6: ATR spectra of the untreated P(OpT70-dBrac)-OPip membrane and the corresponding membrane after alkaline aging for 3 weeks in 2 M KOH solution at 80 °C in the whole spectral region (3700–650 cm^{-1}) and in the magnified region from 1800 to 625 cm^{-1}; Figure S7: ATR spectra of the untreated P(OpT70-dBrac)-Pip membrane and the corresponding membrane after alkaline aging for 3 weeks in 2 M KOH solution at 80 °C in the whole spectral region (3700–650 cm^{-1}) and in the magnified region from 1800 to 625 cm^{-1}.

Acknowledgments

The authors are grateful to M. Kolia (Laboratory of Electron Microscopy and Microanalysis, University of Patras) for TEM measurements.

Author Contributions

Conceptualization, V.D.; Methodology, V.D.; Validation, S.G. and V.D.; Investigation, S.G.; Resources, V.D.; Data Curation, V.D.; Writing—Original Draft Preparation, S.G.; Writing—Review & Editing, V.D.; Visualization, S.G.; Supervision, V.D.

Ethics Statement

Not applicable.

Informed Consent Statement

Not applicable.

Data Availability Statement

Research data are contained within the article and supplementary materials.

Funding

This research was funded by the European Union's Horizon 2020 Research and Innovation Action program "Materials for next generation of alkaline electrolyzer" (NEXTAEC), grant number 862509.

Declaration of Competing Interest

The authors declare that they have no known competing financial interests or personal relationships that could have appeared to influence the work reported in this paper.

References

1. Pivovar B, Rustagi N, Satyapal S. Hydrogen at Scale (H_2@Scale): Key to a Clean, Economic, and Sustainable Energy System. *Electrochem. Soc. Interface* **2018**, *27*, 47–52.
2. Miller HA, Bouzek K, Hnat J, Loos S, Bernäcker CI, Weißgärber T, et al. Green hydrogen from anion exchange membrane water electrolysis: A review of recent developments in critical materials and operating conditions. *Sustain. Energy Fuels* **2020**, *4*, 2114–2133.
3. Brauns J, Turek T. Alkaline Water Electrolysis Powered by Renewable Energy: A Review. *Processes* **2020**, *8*, 248.
4. Li Q, Molina Villarino A, Peltier CR, Macbeth AJ, Yang Y, Kim MJ, et al. Anion Exchange Membrane Water Electrolysis: The Future of Green Hydrogen. *J. Phys. Chem.* **2023**, *127*, 7901–7912.
5. Rocha F, Georgiadis C, Van Droogenbroek K, Delmelle R, Pinon X, Pyka G, et al. Proton exchange membrane-like alkaline water electrolysis using flow-engineered three-dimensional electrodes. *Nat. Commun*. **2024**, *15*, 7444.
6. Deimede V, Labou D, Neophytides SG. Polymer electrolyte membranes based on blends of sulfonated polysulfone and PEO-grafted polyethersulfone for low temperature water electrolysis. *J. Appl. Polym. Sci.* **2014**, *131*, 39922.
7. Carmo M, Fritz DL, Mergel J, Stolten DA. Comprehensive review on PEM water electrolysis. *Int. J. Hydrogen Energy* **2013**, *38*, 4901–4934.
8. Minke C, Suermann M, Bensmann B, Hanke-Rauschenbach R. Is Iridium Demand a Potential Bottleneck in the Realization of Large-Scale PEM Water Electrolysis? *Int. J. Hydrogen Energy* **2021**, *46*, 23581–23590.
9. Li D, Motz AR, Bae C, Fujimoto C, Yang G, Zhang FY, et al. Durability of anion exchange membrane water electrolyzers. *Energy Environ. Sci.* **2022**, *14*, 3393–3419.

10. Henkensmeier D, Cho W-C, Jannasch P, Stojadinovic J, Li Q, Aili D, et al. Separators and Membranes for Advanced Alkaline Water Electrolysis. *Chem. Rev.* **2024**, *124*, 6393–6443.
11. Park EJ, Jannasch P, Miyatake K, Bae C, Noonan K, Fujimoto C, et al. Aryl ether-free polymer electrolytes for electrochemical and energy devices. *Chem. Soc. Rev.* **2024**, *53*, 5704–5780.
12. Jeon JY, Park S, Han J, Maurya S, Mohanty AD, Tian D, et al. Synthesis of aromatic anion exchange membranes by friedel–crafts bromoalkylation and cross-linking of polystyrene block copolymers. *Macromolecules* **2019**, *52*, 2139–2147.
13. Zhu M, Zhang X, Su Y, Wang Y, Wu Y, Yang D, et al. Comb-shaped diblock copolystyrene for anion exchange membranes. *J. Appl. Polym. Sci.* **2015**, *136*, 47370.
14. Dang HS, Jannasch P. Exploring different cationic alkyl side chain designs for enhanced alkaline stability and hydroxide ion conductivity of anion-exchange membranes. *Macromolecules* **2015**, *48*, 5742–5751.
15. Liu L, Chu X, Liao J, Huang Y, Li Y, Ge Z, et al. Tuning the properties of poly(2,6-dimethyl-1,4-phenylene oxide) anion exchange membranes and their performance in H_2/O_2 fuel cells. *Energy Environ. Sci.* **2018**, *11*, 435–446.
16. Zhu Y, Ding L, Liang X, Shehzad MA, Wang L, Ge X, et al. Beneficial use of rotatable-spacer side-chains in alkaline anion exchange membranes for fuel cells. *Energy Environ. Sci*. **2018**, *11*, 3472–3479.
17. Liu L, Ma W, Zhang J, Liu Z, Chu D, Shao R, et al. The design and synthesis of a long-side-chain-type anion exchange membrane with a hydrophilic spacer for alkaline fuel cells. *J. Membr. Sci.* **2023**, *678*, 121663.
18. Zhang J, Ma W, Yin T, Chen S, Zhang X, Li N, et al. Oligo (ethylene glycol)-grafted poly (terphenyl indole piperidinium) with high water diffusivity for anion exchange membrane fuel cells. *J. Membr. Sci.* **2024**, *694*, 122424.
19. Zhang J, Shao R, Yin T, Chu D, Zhang X, Li N, et al. Impact of side chain length on the properties and alkaline fuel cell performance of OEG-grafted poly (terphenyl piperidinium) anion exchange membranes. *J. Membr. Sci.* **2025**, *713*, 123375.
20. Zhang J, Zhang K, Liang X, Yu W, Ge X, Shehzad MA, et al. Self-aggregating cationic-chains enable alkaline stable ion-conducting channels for anion-exchange membrane fuel cells. *J. Mater. Chem*. *A* **2021**, *9*, 327–337.
21. Marino MG, Kreuer KD. Alkaline stability of quaternary ammonium cations for alkaline fuel cell membranes and ionic liquids. *ChemSusChem* **2015**, *8*, 513–523.
22. Park EJ, Kim YS. Quaternized aryl ether-free polyaromatics for alkaline membrane fuel cells: Synthesis, properties, and performance—a topical review. *J. Mater. Chem*. *A* **2018**, *6*, 15456–15477.
23. Akiyama R, Yokota N, Miyatake K. Chemically stable, highly anion conductive polymers composed of quinquephenylene and pendant ammonium groups. *Macromolecules* **2019**, *52*, 2131–2138.
24. Olsson JS, Pham TH, Jannasch P. Functionalizing Polystyrene with N-Alicyclic Piperidine-Based Cations via Friedel–Crafts Alkylation for Highly Alkali-Stable Anion-Exchange Membranes. *Macromolecules* **2020**, *53*, 4722–4732.
25. Allushi A, Bakvand PM, Jannasch P. Polyfluorenes bearing N, N-dimethylpiperidinium cations on short spacers for durable anion exchange membranes. *Macromolecules* **2023**, *56*, 1165–1176.
26. Liu M, Hu X, Hu B, Liu L, Li N. Soluble poly (aryl piperidinium) with extended aromatic segments as anion exchange membranes for alkaline fuel cells and water electrolysis. *J. Membr. Sci.* **2022**, *642*, 119966.
27. Hu X, Hu B, Niu C, Yao J, Liu M, Tao H, et al. An operationally broadened alkaline water electrolyser enabled by highly stable poly(oxindole biphenylene) ion-solvating membranes. *Nat. Energy* **2024**, *9*, 401–410.
28. Gjoshi S, Loukopoulou P, Plevova M, Hnat J, Bouzek K, Deimede V. Cycloaliphatic Quaternary Ammonium Functionalized Poly(oxindole biphenyl) Based Anion-Exchange Membranes for Water Electrolysis: Stability and Performance. *Polymers* **2024**, *16*, 99.
29. Makrygianni M, Aivali S, Xia Y, Kraglund MR, Aili D, Deimede V. Polyisatin derived ion-solvating blend membranes for alkaline water electrolysis. *J. Membr. Sci.* **2023**, *669*, 121331.
30. He T, Shen R, Lin C, Zhu A, Xie Z, Zhang Q. Poly (isatin-co-biphenyl alkylene) anion exchange membranes with fluorinated side chains and pendant cationic groups for water electrolysis. *J. Membr. Sci.* **2025**, *728*, 124148.
31. Wang K, Gao L, Liu J, Su X, Yan X, Dai Y, et al. Comb-shaped ether-free poly(biphenyl indole) based alkaline membrane. *J. Membr. Sci*. **2019**, *588*, 117216.
32. Gjoshi S, Anastasopoulos C, Ghotia K, Grilli D, Egert F, Ansar SA, et al. Tuning Properties of PEO-Functionalized Ion-solvating Blend Membranes via PEO side chain length: Impact on alkaline water electrolysis performance. *J. Membr. Sci.* **2025**, *733*, 124368.
33. Katsaiti M, Gjoshi S, Deimede V, Manariotis ID, Kallitsis JK, Mantzavinos D, et al. An optimized Zn-air battery using a polymer-blend anion transfer membrane and a biochar electrocatalyst. *Electrochim. Acta* **2025**, *532*, 146510.
34. Zhang S, Zhu X, Jin C. Development of high-performance anion exchange membrane fuel cell using poly(isatin biphenylene) with flexible heterocycle quaternary ammonium cations. *J. Mater. Chem*. *A* **2019**, *7*, 6883–6893.
35. Long C, Zhao T, Tian L, Liu, Q, Wang F, Wang Z, et al. Highly stable and conductive multicationic poly(biphenyl indole) with extender side chains for anion exchange membrane fuel cells. *ACS Appl. Energy Mater.* **2021**, *4*, 6154−6165.
36. Yin Z, Wu Y, Shi B, Yang C, Kong Y, Liu Y, et al. Alkaline stable piperidinium-based biphenyl polymer for anion exchange membranes. *Solid State Ion.* **2022**, *383*, 115969.

37. Wang Y, Wang S, Sui Z, Gu Y, Zhang Y, Gao J, et al. "Fishbone" Design of Amino/N-Spirocyclic Cations Toward High-Performance Poly (triphenylene piperidine) Anion-Exchange Membranes for Fuel Cells. *ACS Appl. Mater. Interfaces* **2024**, *16*, 4003–4012.
38. Nieto DR, Fomine S, Zolotukhin MG, Fomina L, Hernandez MCG. Superelectrophilic Activation of N-Substituted Isatins: Implications for Polymer Synthesis, a Theoretical Study. *Macromol. Theory Simul*. **2009**, *18*, 138–144.
39. Hernandez MCG, Zolotukhin MG, Fomine S, Cedillo G, Morales SL, Fröhlich N, et al. Novel, metal-free, superacid-catalyzed "click" reactions of isatins with linear, nonactivated, multiring aromatic hydrocarbons. *Macromolecules* **2010**, *43*, 6968–6979.
40. Afsar NU, Erigene B, Irfan M, Wu B, Xu T, Ji W, et al. High performance anion exchange membrane with proton transport pathways for diffusion dialysis. *Sep. Purif. Technol.* **2018**, *193*, 11–20.
41. Papakonstantinou P, Deimede V. Self-cross-linked quaternary phosphonium based anion exchange membranes: Assessing the influence of quaternary phosphonium groups on alkaline stability. *RSC Adv*. **2016**, *6*, 114329–114343.
42. Tsagdi A, Dimitriou M, Druvari D, Deimede V. Blend membranes based on N1-alkyl-substituted imidazolium functionalized polymers and aromatic polyethers: influence of N1-alkyl substituent on properties and alkaline stability. *Polym. Bull.* **2022**, *79*, 1647–1668.
43. Ioannidi A, Vroulias D, Kallitsis J, Ioannides T, Deimede V. Synthesis and characterization of poly(ethylene oxide) based copolymer membranes for efficient gas/vapor separation: Effect of PEO content and chain length. *J. Membr. Sci.* **2021**, *632*, 119353.
44. Yu W, Zhang J, Liang X, Ge X, Wei C, Ge Z, et al. Anion exchange membranes with fast ion transport channels driven by cation-dipole interactions for alkaline fuel cells. *J. Membr. Sci.* **2021**, *634*, 119404.
45. Li L, Wang J, Hussain M, Ma L, Qaisrani NA, Ma S, et al. Side-chain manipulation of poly (phenylene oxide) based anion exchange membrane: Alkoxyl extender integrated with flexible spacer. *J. Membr. Sci.* **2021**, *624*, 119088.
46. Hu X, Huang Y, Liu L, Ju Q, Zhou X, Qiao X, et al. Piperidinium functionalized aryl ether-free polyaromatics as anion exchange membrane for water electrolysers: Performance and durability. *J. Membr. Sci.* **2021**, *621*, 118964.
47. Wang Y, Zhao BP, Setzler S, Rojas-Carbonell C, Ben Yehuda A, Amel M, et al. Poly(aryl piperidinium) membranes and ionomers for hydroxide exchange membrane fuel cells. *Nat. Energy* **2019**, *4*, 392–398.
48. Zhang J, Yu W, Liang X, Zhang K, Wang H, Ge X, et al. Flexible bis-piperidinium side chains construct highly conductive and robust anion-exchange membranes. *ACS Appl. Energy Mater.* **2021**, *4*, 9701–9711.
49. He Y, Pan J, Wu L, Zhu Y, Ge X, Ran J, et al. A Novel Methodology to Synthesize Highly Conductive Anion Exchange Membranes. *Sci. Rep*. **2015**, *5*, 13417.
50. Aili D, Kraglund MR, Rajappan SC, Serhiichuk D, Xia Y, Deimede V, et al. Electrode Separators for the Next-Generation Alkaline Water Electrolyzers. *ACS Energy Lett.* **2023**, *8*, 1900–1910.
51. Chen S, Xia Y, Aili D, Jannasch P. Influence of highly flexible di (biphenyl) ethane units on the properties of poly (arylene piperidinium) anion exchange membranes. *J. Mater. Chem. A* **2025***,* https://doi.org/10.1039/D5TA04171F.
52. Boström O, Choi SY, Xia L, Meital S, Lohmann-Richters F, Jannasch P. Alkali-stable polybenzimidazole anion exchange membranes tethered with N,Ndimethylpiperidinium cations for dilute aqueous KOH fed water electrolyzers. *J. Mater. Chem. A* **2023**, *11*, 21170–21182.
53. Peng Z, Liu X, Wang Q, Zhao Y, Jannasch P, Yang J. Anion exchange membranes based on Poly (oxindole biphenylene) grafted with hydroxyl and quaternary ammonium groups for alkaline water electrolysis. *Mater. Today Chem.* **2025**, *44*, 102579.
54. Ren R, Zhang S, Miller HA, Vizza F, Varcoe JR, He Q. Facile preparation of novel cardo Poly(oxindolebiphenylylene) with pendent quaternary ammonium by superacid-catalysed polyhydroxyalkylation reaction for anion exchange membranes. *J. Membr. Sci*. **2019**, *591*, 117320.
55. Allushi A, Pham TH, Olsson JS, Jannasch P. Ether-free polyfluorenes tethered with quinuclidinium cations as hydroxide exchange membranes. *J. Mater. Chem. A* **2019**, *7*, 27164–27174.